Design of operator-based low power recording system for detecting contact signals from triboelectric touch sensor

Joon Young Lim[1, †], Seo Kwon Joo[1, †], Gyu Ri Kim[2], Chae Eun Lee[1], Yu Ri Kim[1], and Yoon Kyu Song[a]

[1, a] Graduate School of Convergence Science and Technology, Seoul National University

[2] Department of Biomedical Engineering, Kyunghee University

E-mail: [1]limjoony@snu.ac.kr

[†] These authors contributed equally to this work

***Abstract* - This paper proposes a triboelectric nanogenerator (TENG) touch sensor combined with a spike detecting system capable of recognizing minute touches. Considering the characteristics of wearable and tactile-based architectures in TENG devices, the low power consumption and small implementation area of the IC are required. A non-linear energy operator which is used for the spike detection system replaces the digital logic with additional circuits and avoids the need for additional circuitry for signal processing. The resulting recording system built in a standard 180 nm CMOS technology can measure the signal from 0.1 Hz to 7 kHz, meanwhile, detect spikes generated by the TENG device. The system has a supply voltage under 1.2 V and powers 22.56 μW while maintaining an acceptable noise level and a total IC area of 1 mm × 1 mm, including input-output pads.**

***Keywords*—Non-linear energy operator (NEO), Spike detection, Touch sensors, Triboelectric nanogenerators (TENG)**

I. INTRODUCTION

The triboelectric nanogenerator (TENG) is an energy harvesting device driven by triboelectrification and electrostatic induction. TENGs have high output voltage, high efficiency, low cost, and easy manufacturing. TENG can be classified into several modes by the direction of polarization change and electrode configuration [1]. Among them, the single-electrode mode TENG acts as a friction layer for only one electrode, while the other acts as a potential reference. When the object approaches or detaches from the electrode, the local electric field distribution changes and electron exchange occurs between the lower stage electrode and the reference electrode or grounds to maintain a balanced potential [2]. Unlike other modes of TENG, this mode has the advantage of using a single electrode to reduce system limitations and complexity and increase flexibility [3]. It is also advantageous for detecting contact with foreign substances because it does not require electrodes to be connected to moving parts.

Due to these features, many studies have utilized single-electrode mode TENG as a touch sensor. In the single-electrode mode TENG touch sensor, when the finger touches the active area of the TENG, electrons move from the finger to friction layer and cause polarization. Then the contact-separation of the finger occurs the electron exchange between electrode-ground to make the net charge of the system zero. The single-electrode mode TENG touch sensors were fabricated by the intaglio contact printing method [4]. The CNT composite was patterned and used as an electrode. Because the advantage of this patterning method that is not limited to a substrate, a CNT electrode can be printed on a perfluoroalkyl alkanes (PFA) film having low surface energy. PFA with a high negative charge affinity can increase the TENG output by accepting many electrons from the finger.

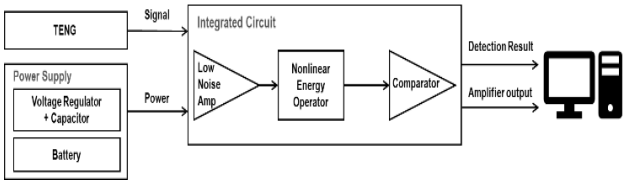

Fig. 1. Schematic diagram of NEO calculation spike detection system.

As shown in Figure 1, the system utilizes the spike detection algorithm that implements the Non-linear Energy Operator through analog calculations and adopts the structure of detecting spikes through the corresponding operator. The spike format output of this algorithm is applied to measure the triboelectric power of TENG with a short peak duration as a signal. This lightweight, low-power detection system is required to combine the TENG touch sensor with wearable and tactile sensors in the future. Therefore, we perform detection differently from the detection method using a comparator in this system. When implementing a Non-linear Energy Operator, signal strength, variation, and frequency components are considered. Through these, it has a robust property of low-frequency high amplitude noise because it detects by additionally considering the frequency change of the short moment of the spike. Finally, to configure a low-power system, we record the signal generated by the TENG element using a low-power analog amplifier operating at 1.2 V and introduce a spike detecting method utilizing an operator to configure the sensor effectively.

In this paper, a 1.2 V electrical sensor microsystem is designed and tested for the TENG touch sensor. Based on the measured results of the TENG pattern, we designed the spike detection circuit. Then utilizing the derived current, the system can measure the presence and the pressure of the contact, which are mathematically calculated. Finally, the quantitative relationship between the contact area and pressure is analyzed.

a. Corresponding author; songyk@snu.ac.kr

Manuscript Received May. 25, 2022, Revised Oct. 19, 2022, Accepted Oct. 20, 2022

Ⅱ. EXPERIMENTS

A. Fabrication of TENG touch sensor

Fig. 2. (a) shows the optical image of the fabricated CNT composite electrodes for the TENG touch sensor. The fabrication of a CNT/paraffin composite-based single-mode TENG touch sensor was followed by the methods in our previous report [4]. The PDMS stamps were prepared with an intaglio pattern and the CNT composite with 5 wt% CNT contents in paraffin solvent. The molten CNT composite on the hot plate (> 70 ℃) is put into the intaglio space of the PDMS stamp. The composite could be transferred to the PFA film as solidified on it. Then, the pattern side was attached to the glass substrate with gentle heating while connecting copper wire.

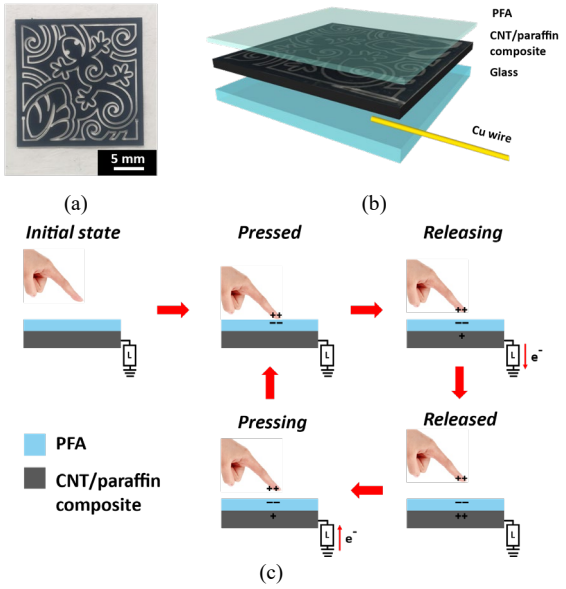

Fig. 2. (a) Optical image of the TENG device. (b) Structure of the patterned CNT composite-based TENG device. (c) Mechanism of the TENG touch sensor.

With the intaglio contact printing, it can be printed in various shapes. Fig. 2. (b) shows the structure of the TENG touch sensor. The CNT electrode is printed on the backside of the PFA film and fixed to the glass substrate for touch. PFA is a frictional layer that accepts electrons from the finger. The mechanism of the TENG touch sensor is shown in Fig. 2. (c). After the initial state, electrons move from the skin to the PFA film (triboelectrification) when the finger touches the PFA film. After that, electrons move between the lower electrode and the ground to set the net charge of the system to zero as the fingers contact and separate (electrostatic induction).

B. Spike Detection System Design

The analog front end of the system includes a fully differential operational amplifier with a feedback capacitor in Fig. 3. (a) and a feedback subthreshold MOS resistor in two cascading stages to amplify and filter the signal. Since the noise characteristics of the analog amplifier are transmitted to the next stage and have a binding effect, the noise figure according to the structural characteristics of the amplifier is an issue that needs to be carefully considered.

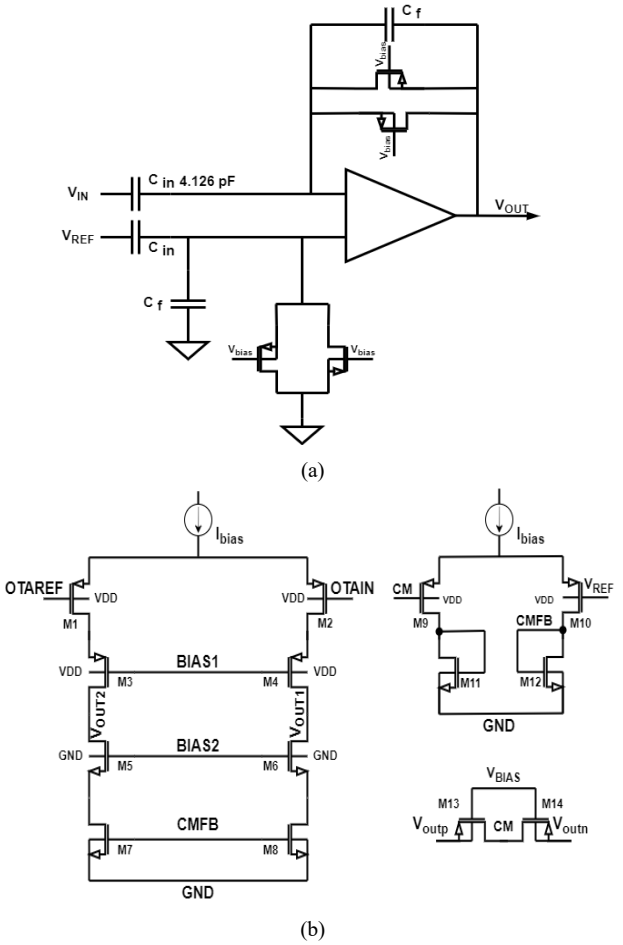

Fig. 3. (a) Top-level diagram of the capacitive-feedback amplifier. (b) The amplifier circuit

A complementary input reduces the input-referred noise, and a telescopic arrangement of components is used to obtain a higher gain, detailed structure of the pre-amplifier is shown at Fig. 3. (b). This topology is suitable for driving capacitive loads and minimizing noise, with each transistor designed to operate in the weak, moderate, or strong inversion region. The common-mode feedback (CMFB) circuit is implemented to stabilize the output voltage by adjusting the common-mode output current. Further stabilization of the output voltage is induced by cascade structure. Detailed design variables for amplifier design is shown at Table I.

TABLE I. Design values of the amplifier.

Devices	W / L (μm)
M1, M2	220 / 1
M3, M4	8 / 2
M5, M6	19.3 / 0.5
M7, M8	2.5 / 8
M9, M10	30 / 1
M11, M12	0.36 / 15
M13, M14	0.22 / 19
M_R	0.22 / 19

The pseudo-resistor structure is based on the symmetrical biasing of the body and gate of two NMOS transistors under the subthreshold operating region. The circuit can utilize very high resistance values of tens of tera-ohms by using the simple architecture. The pseudo-resistor used in the circuit showed $r_{inc} > 10^{12}\,\Omega$, and the input capacitor C_{in} is 4.126 pF. The amplifier bandwidth achieved 0.2 Hz – 7 kHz. The specification of designed amplifier is listed in following Table II.

TABLE I. Amplifier Specification

Specification	Values
Supply voltage	1.2 V
Power Consumption	7.32 μW
Total Gain	35 dB
Bandwidth	0.2 Hz ~ 7 kHz
CMRR	70 dB
PSRR	80 dB
Input referred noise	5.4 μVrms

Non-linear energy operator (NEO) have already been used to compute signals' instantaneous frequency and amplitude [5]–[10]. It is superior to other detection methods for spike detection in low signal-to-noise environments [11], [12]. The circuit is relatively simple and can be implemented on a large-scale implantable chip. The NEO is defined as

$$\varphi(x(t)) = \left(\frac{dx(t)}{dt}\right)^2 - x(t)\frac{d^2x(t)}{dt^2} \quad (1)$$

Where the $x(t)$ is the continuous analog input signal. Since the frequency component is extracted in the derivative, the low-frequency components are attenuated, and the high-frequency components are emphasized. Thus, the NEO-based detection system is robust against low-frequency, high-amplitude noise.

The non-linear energy operator of the input signal is implemented through analog calculation, and the corresponding operator in the system detects the spike. The circuit consists of an analog differentiator, multiplier, and subtractor to perform the analog calculation using a low power design. The proposed CMOS circuits can achieve very low power based on the sub-threshold region, where $V_{GS} < V_{TH}$, the MOS transistor provides a minimum saturation voltage of $V_{DS} = 4\sim5\ V_T$ with a very low drain current [13].

TABLE II. Design values of the differentiator

Devices	W / L (μm)
M0, M1, M2, M3	2 / 2
M4, M7	0.26 / 12.4
M5, M6	20 / 1

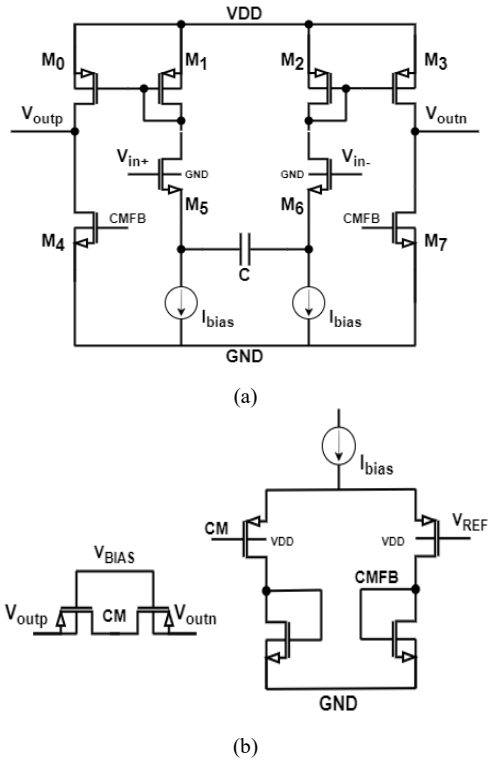

Fig. 4. The schematic of the (a) differentiator and (b) CMFB with a differential structure

The differentiation circuit uses the capacitor's current-voltage relationship, where the voltage applied to the capacitor indicates the current charging the capacitor.

$$I = C\frac{dv}{dt} \quad (2)$$

Where I is instantaneous current across the capacitor, C is capacitance, and dv/dt is the voltage change rate across the capacitor.

Instantaneous current, the amount of current at a specific point in time, is expressed as an instantaneous voltage change with time or a rate of voltage change at a particular point in time. From a physical point of view, an increasing voltage across the capacitor is induced by a charge difference across the capacitor plates. Therefore, there must be a steady charge rate on the capacitor for a constant voltage increase, which equals a continuous current flow. Fig. 4. (a) shows a differentiator design based on the relationship between voltage and current on the capacitor.

The fully differential structure is applied to the differentiator. The CMFB circuit in Fig. 4. (b) is implemented to the differentiator for the stable common-mode voltage used in the following analog calculation stages. The current source for the differentiator is realized using a high impedance cascade current sink. The supply voltage of the differentiator is $V_{DD} = 1.2$ V, and the reference voltage in CMFB is $V_{ref} = 0.6$ V. The differentiator can achieve a low current consumption of 0.245 μA, including the feedback circuit.

The four-quadrant multiplier in Fig. 5. operating in the subthreshold region is designed based on the body-drain-

connected structure. The sub-threshold multiplier uses a cross-coupled quadrant input structure driven by the gate and bulk of four PMOS devices to obtain differential multiplication. This topology achieves a higher input range than CMOS implementations of small Gilbert multipliers [14].

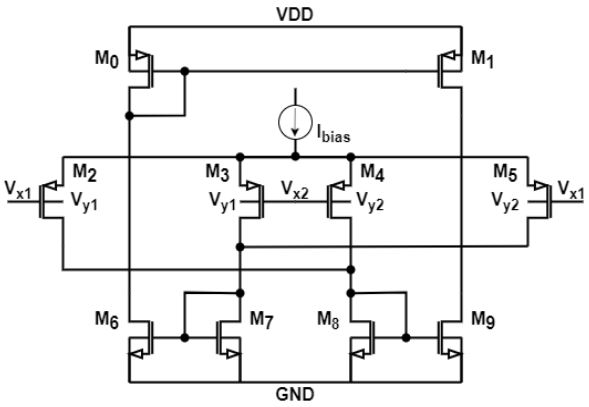

Fig. 5. Subthreshold four-quadrant multiplier using gate and body input

TABLE III. Design values of the multiplier

Devices	W / L (μm)
M0	5 / 5
M1	4.9 / 5
M2, M3, M4, M5	0.22 / 5
M6, M7, M8, M9	1 / 1

M2, M3, M4, and M5 operate in the subthreshold region, and the output current can be approximated to a first-order equation. In a MOS transistor, the sub-threshold drain-source current is driven by the equation below [9], [13].

$$I_{ds} = I_s \cdot exp\ exp\left([1-k]\cdot\frac{V_{bs}}{V_t}\right)\cdot exp\left(k\cdot\frac{V_{gs}}{V_t}\right)\cdot \left(1-exp\left(-\frac{V_{ds}}{V_t}\right)+\frac{V_{ds}}{V_o}\right) \quad (3)$$

Where, I_s is the width-length raito compensated characteristic current, V_{bs} is the body-source potential, V_{gs} is the gate-source potential, V_{ds} is the drain-source potential, k is the effectiveness constant of the channel current controlling gate, $V_t = kT/q$, and V_o is the Early voltage.

By the condition of $V_{ds} \geq 4 \cdot V_t$ in the quiescent reverse-biased operation of the MOS transistor and negligent Early effect, the output current, I_{OUT} is obtained in the reverse-biased MOS transistor as follows

$$I_{OUT} = (I_3 + I_4) - (I_1 + I_2) = \frac{I_{bias}\cdot k\cdot(1-k)}{4\cdot V_t}\cdot V_1 \cdot V_2 \quad (4)$$

While V_1 , $V_2 \leq V_t/k$, the effectiveness constant is reciprocal to the slope factor (≈0.6 in the CMOS process), and the multiplier operates in the linear range [6]. The output current is proportional to the V_1, V_2.

The voltage adder/subtractor in Fig. 6 consists of two symmetric subcircuits, in which its inputs are balanced with reference bias voltage.

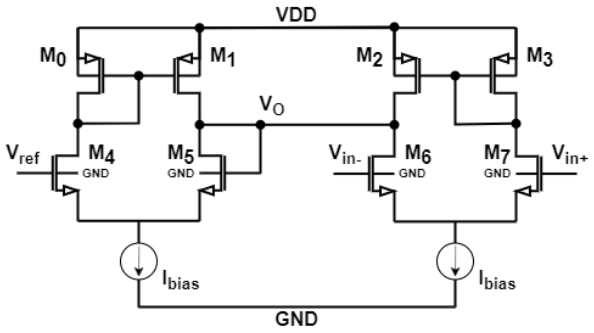

Fig. 7. The simple voltage adder/subtractor

TABLE V. Design values of the differentiator.

Devices	W / L (μm)
M0, M1, M2, M3	5 / 5
M4, M6, M7	2 / 10
M5	10 / 2

The addition and subtraction of differential input signals are implemented using analog adders in Fig. 6. The current subtractor operates at the saturation region. To keep M4 operating in the saturation region, V_{GS} should be larger than $V_{T,}$ and V_{GD} should be less than V_T for M4.

The comparator evaluates the detected spiking event signal and digitizes it into binary data according to internal bias. The event signal is transmitted to external devices and further processed to be utilized.

Ⅲ. RESULTS AND DISCUSSIONS

As shown in Fig. 7. (a), the layout of the core IC occupies a 1 mm × 1 mm area. Fig. 7. (b) shows the microphotograph of the fabricated IC. The operator calculation spike detecting module occupies 262 μm × 145 μm. The fabrication of the system is done on TSMC 180 nm RFCMOS process.

The IC was mounted on the custom-designed PCB test board, using 4 copper layers and stitching vias to minimize noise figures. The output signals were obtained through an SMA connector and cable, and the input TENG signal was wired to the input pad of the board.

Fig. 7. (c) shows the experimental test board uses a battery as a power source and controls the voltage using a commercial 1.2 V regulator and matching 1 μF caps. The output of the amplifier and spike detection result is measured by the oscilloscope (Keysight MSOX3024T). The surrounding was shielded by a grounded Faraday cage, and each instrument's ground was connected by wires. Still, there exists 60 Hz noise produced by the commercial AC supply, generating minor turbulence on the amplifier output and detecting measurements.

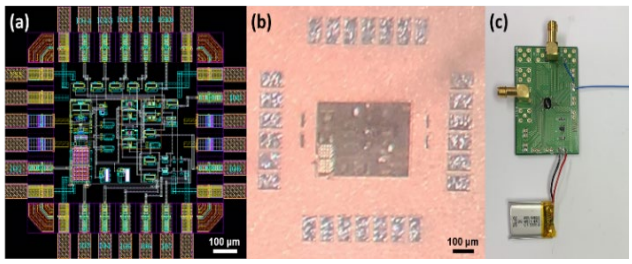

(a) (b) (c)

Fig. 8. (a) Layout of the system. (b) Microphotograph of fabricated IC in TSMC 180 nm RFCMOS process. (c) Experimental test board setup.

As TENG produces different currents depending on pressure, an experiment is conducted first to derive a current generation relationship according to pressure. The TENG device is fixed on the electronic scale (Hansung HS2140A) and repeatedly tapped to verify the relationship between the touching pressure and the produced current. The signal generated by the device is recorded by the oscilloscope, and the scale value while applying pressure was recorded.

The measurement results are shown in Fig. 8. (a). The current waveforms generated when a force of 0.01, 0.05, 0.10, and 0.15 N was applied to TENG were recorded. A spike-shaped voltage peak in first contact of the finger and a relatively small recovery negative voltage peak were observed. The induced voltage peak was characterized by repeated trials.

Fig. 8. (b) shows the statistical data of produced peak voltage based on the pressuring force and displays the output voltage's proportional increase as the pressure increases. Depending on the contact area, the current generated by the TENG device is also compared; the detailed data is in supplementary figures. The touching area increase also leads to the output voltage increase.

The output of the system's amplifier and the spike detection result were also recorded. Fig. 8. (c) shows the raw TENG input connected to the system, the amplifier output of the system, and the spike detection result of the NEO operator calculation module. The resistance between the test board input pad and ground was 35.6 kΩ, lower than the amplifier's input impedance. The low resistance between the test board input and the ground attenuated the signal amplitude, affecting amplifier output and input signal measurement. The oscilloscope probe has a 10 MΩ input impedance while the pad has 35.6 kΩ to the ground, and the current produced by the device favors leaking to the ground. Since the TENG output is a current-based signal, the output peak voltage measured by the oscilloscope directly on the test-board input pad is reduced. To measure the TENG device output voltage signal simultaneously with amplifier output and detection result, a 2.2 MΩ resistor was applied to the input pad of the test board. In this manner, the signal connected to the system became recordable by the oscilloscope.

The amplifier output value was then connected to the system in the IC and used for spike detection. The input from the TENG device passes through the amplifier and the NEO calculation circuit, and spike detection is performed using the comparator.

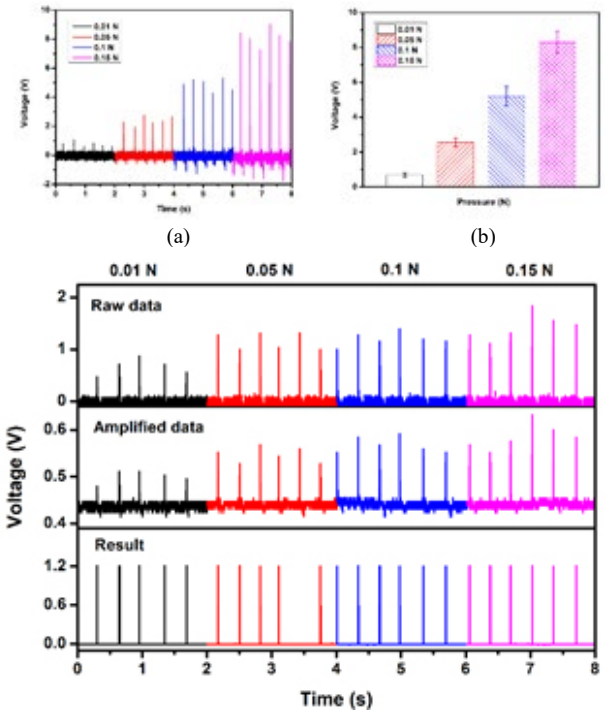

(c)

Fig. 9. (a) The output of the TENG device based on the tapping pressure. (b) The relationship between tapping pressure and the voltage output. (c) The detecting system input, amplifier output, and detecting result.

IV. CONCLUSION

This paper presented the spike detecting analog front end applied to the spike-shaped current generating device, TENG. Spike detection is a way of sensing, with NEO being relatively robust to ambient noise, considering frequency more specific to instantaneous high spike signals. The system consumed 22.56 μW of power and occupied 1 mm × 1 mm of IC area. Compared to the commercial comparator-based simple detectors, the system had low power consumption and size advantages with noise-tolerant detection functions. As the broad aim of this system was a wearable device, a wireless transceiver for power and data transmission would serve extensive device. Since the TENG works as an energy harvesting device, the system could be driven using power generated by TENG in further research. Also, the signal detection is conducted by a single chip without other off-chip components, which minimizes the system size.

ACKNOWLEDGMENT

This research was supported by the Bio & Medical Technology Development Program of the National Research Foundation (NRF) & funded by the Korean government (MSIT) (2022M3E5E9016884). Also, the chip fabrication and EDA tool were supported by the IC Design Education Center(IDEC), Korea.

REFERENCES

[1] C. Wu, A. C. Wang, W. Ding, H. Guo, and Z. L. Wang, "Triboelectric Nanogenerator: A Foundation of the Energy for the New Era," *Adv. Energy Mater.*, vol. 9, no. 1, pp. 1–25, 2019, doi: 10.1002/aenm.201802906.

[2] S. Wang, L. Lin, and Z. L. Wang, "Triboelectric nanogenerators as self-powered active sensors," *Nano Energy*, vol. 11, pp. 436–462, 2015, doi: 10.1016/j.nanoen.2014.10.034.

[3] W. Ding, A. C. Wang, C. Wu, H. Guo, and Z. L. Wang, "Human–Machine Interfacing Enabled by Triboelectric Nanogenerators and Tribotronics," *Adv. Mater. Technol.*, vol. 4, no. 1, pp. 1–16, 2019, doi: 10.1002/admt.201800487.

[4] S. Joo, C. E. Lee, J. Kang, S. Seo, Y. K. Song, and J. H. Kim, "Intaglio Contact Printing of Versatile Carbon Nanotube Composites and Its Applications for Miniaturizing High-Performance Devices," *Small*, vol. 18, no. 3, pp. 1–10, 2022, doi: 10.1002/smll.202106174.

[5] J. F. Kaiser, "On a simple algorithm to calculate the 'energy' of a signal," *ICASSP, IEEE Int. Conf. Acoust. Speech Signal Process. - Proc.*, vol. 1, no. 10, pp. 381–384, 1990, doi: 10.1109/icassp.1990.115702.

[6] B. Gosselin and M. Sawan, "An ultra low-power CMOS automatic action potential detector," *IEEE Trans. Neural Syst. Rehabil. Eng.*, vol. 17, no. 4, pp. 346–353, 2009, doi: 10.1109/TNSRE.2009.2018103.

[7] Y. G. Li, Q. Ma, M. R. Haider, and Y. Massoud, "Ultra-low-power high sensitivity spike detectors based on modified nonlinear energy operator," *Proc. - IEEE Int. Symp. Circuits Syst.*, pp. 137–140, 2013, doi: 10.1109/ISCAS.2013.6571801.

[8] E. Koutsos, S. E. Paraskevopoulou, and T. G. Constandinou, "A 1.5 μw NEO-based spike detector with adaptive-threshold for calibration-free multichannel neural interfaces," *Proc. - IEEE Int. Symp. Circuits Syst.*, pp. 1922–1925, 2013, doi: 10.1109/ISCAS.2013.6572243.

[9] W. Cao and H. Li, "Ultra-low-power neural recording microsystem for implantable brain machine interface," *Proc. - 2013 IEEE Int. Conf. Green Comput. Commun. IEEE Internet Things IEEE Cyber, Phys. Soc. Comput. GreenCom-iThings-CPSCom 2013*, pp. 1050–1053, 2013, doi: 10.1109/GreenCom-iThings-CPSCom.2013.178.

[10] J. P. Kim, H. Lee, and H. Ko, "0.6 V, 116 nW neural spike acquisition IC with self-biased instrumentation amplifier and analog spike extraction," *Sensors (Switzerland)*, vol. 18, no. 8, pp. 1–13, 2018, doi: 10.3390/s18082460.

[11] S. Mukhopadhyay and G. C. Ray, "A new interpretation of nonlinear energy operator and its efficacy in spike detection," *IEEE Trans. Biomed. Eng.*, vol. 45, no. 2, pp. 180–187, 1998, doi: 10.1109/10.661266.

[12] I. Obeid and P. D. Wolf, "Evaluation of spike-detection algorithms for a brain-machine interface application," *IEEE Trans. Biomed. Eng.*, vol. 51, no. 6, pp. 905–911, 2004, doi: 10.1109/TBME.2004.826683.

[13] E. Vittoz and J. Fellrath, "CMOS Analog Integrated Circuits Based on Weak Inversion Operation," *IEEE J. Solid-State Circuits*, vol. 12, no. 3, pp. 224–231, 1977, doi: 10.1109/JSSC.1977.1050882.

[14] G. Han and E. Sánchez-Sinencio, "CMOS transconductance multipliers: A tutorial," *IEEE Trans. Circuits Syst. II Analog Digit. Signal Process.*, vol. 45, no. 12, pp. 1550–1563, 1998, doi: 10.1109/82.746667.

Joon Young Lim received a B.S. degree in Nanoscience Engineering from Yonsei University, Seoul, Korea, in 2020 and is currently working toward Integrated M.S. and Ph.D. degree at Seoul National University, Korea.

His main interest is designing and applying functional-analog front-end in the Brain-Machine Interface system.

Seok Won Joo received a B.S. and M.S. degree in nano-engineering from Gachon University, Seongnam, Korea, in 2016.

His main interest is the fabrication of microstructures via various lithography techniques and applying it to electrical devices.

Gyu Ri Kim currently studies in Department of Biomedical Engineering, Kyunghee University, Gyeonggi 17104, Korea.

Her main interests are RF circuits for wireless communications, especially highly efficient and linear RF transmitters.

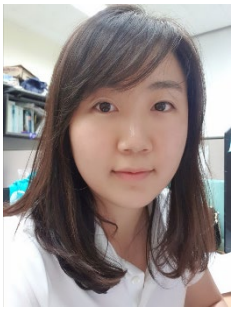

Chae Eun Lee received a B.S degree in Electronics Engineering from Ewha Womans University, in 2017 and is currently working toward a Ph.D. degree in Nanoscience and Technology from Seoul National University, Korea.

Her research interests include developing neuromodulation devices for visual prosthesis and bidirectional implantable Brain-Machine interfaces.

Yu Ri Kim received a B.S. degree in Electric Engineering from Soongsil University, Seoul, Korea, in 2018 and is currently working toward Master degree in Nanoscience and Technology from Seoul National University, Korea.

Her research interests include designing ultra-low-power systems for Brain-Machine Interface and recording Bio-Impedance.

Yoon Kyu Song received the B.S. and M.S. degree in Electric engineering from Seoul National University, Korea, in 1992 and 1994, respectively, and the Ph.D. degree from Brown University, Providence, RI, in 1999.

His research interests include basic and applied semiconductor optoelectronics, such as vertical-cavity lasers and nanostructured light emitters.